

Metallicity effects on the chromospheric activity–age relation for late-type dwarfs

H. J. Rocha-Pinto and W. J. Maciel

Instituto Astronômico e Geofísico, Av. Miguel Stefano 4200, 04301-904 São Paulo, Brazil

Accepted 1998 February 21. Received 1998 February 19; in original form 1997 December 23

ABSTRACT

We show that there is a relationship between the age excess, defined as the difference between the stellar isochrone and chromospheric ages, and the metallicity as measured by the index $[\text{Fe}/\text{H}]$ for late-type dwarfs. The chromospheric age tends to be lower than the isochrone age for metal-poor stars, and the opposite occurs for metal-rich objects. We suggest that this could be an effect of neglecting the metallicity dependence of the calibrated chromospheric emission–age relation. We propose a correction to account for this dependence. We also investigate the metallicity distributions of these stars, and show that there are distinct trends according to the chromospheric activity level. Inactive stars have a metallicity distribution which resembles the metallicity distribution of solar neighbourhood stars, while active stars appear to be concentrated in an activity strip on the $\log R'_{\text{HK}} \times [\text{Fe}/\text{H}]$ diagram. We provide some explanations for these trends, and show that the chromospheric emission–age relation probably has different slopes on the two sides of the Vaughan–Preston gap.

Key words: stars: activity – stars: chromospheres – stars: fundamental parameters – stars: late-type.

1 INTRODUCTION

The usual method for estimating ages of field stars consists of comparing the star position, in an $M_V \times \log T_{\text{eff}}$ diagram, with respect to a grid of theoretical isochrones. This procedure is affected by errors in both coordinates, although the uncertainties in the determination of the bolometric corrections and effective temperatures are particularly important.

An alternate method, which seems to be very promising for estimating ages in late-type dwarfs, makes use of the chromospheric emission (CE) in these stars. From the pioneering work by Wilson (1963), there is much evidence in the literature that the stellar chromospheric activity can be associated with the stellar age (e.g. Skumanich 1972; Barry, Cromwell & Hege 1987; Eggen 1990; Soderblom, Duncan & Johnson 1991). According to these investigations, young stars show CE levels systematically higher than the older stars.

Recently, Henry et al. (1996, hereafter HSDB) published the results of an extensive survey of CE in southern hemisphere G dwarfs. These data, together with the data previously published by Soderblom (1985), make possible the study of the CE in a large number of stars with varying ages and chemical compositions. This work attempts to discuss the estimate of stellar ages using chromospheric indices in stars with different chemical compositions. In Section 2, we make a comparison between isochrone and chromospheric ages, and show that the chromospheric ages present systematic deviations related to the isochrone ages, as a function of the metallicity $[\text{Fe}/\text{H}]$. In Section 3, we study the differences in the

metallicity distributions of the active and inactive stars, and show that the active stars seem to be located in a strip in the CE–metallicity diagram. In Section 4 we give some explanations for this strip and for other trends in the diagram. Finally, the CE–age relation on both sides of the Vaughan–Preston gap is treated in Section 5.

2 A COMPARISON OF ISOCHRONE AND CHROMOSPHERIC AGES

Soderblom et al. (1991) demonstrated that the CE level, as measured by the index $\log R'_{\text{HK}}$, is directly related to the stellar age. This relation is not a statistical one, but a deterministic relation, the form of which has not been well determined. Because of the scatter in the data, Soderblom et al. decided not to choose between a simple power-law calibration, which would produce many very young stars, and a more complicated calibration which would preserve the constancy of the star formation rate.

Also, they argued that the relation between CE and stellar age seems to be independent of $[\text{Fe}/\text{H}]$, as the Hyades and Coma clusters show the same CE levels and have the same age, although with different chemical compositions. In spite of that, Soderblom et al. acknowledge that low metallicity stars should have a different CE–age relation, since in these stars the Ca II H and K lines are intrinsically shallower than in solar metallicity stars. In this sense, old metal-poor stars would resemble very young stars due to a higher $\log R'_{\text{HK}}$.

To investigate the metallicity dependence of the chromospheric activity–age relation, we have used the recent data base by

Edvardsson et al. (1993, hereafter Edv93), which comprises mainly late F and early G dwarfs. Since the surveys of HSDB and Soderblom (1985) include mainly G dwarfs, only a fraction of the stars in the Edv93 sample have measured chromospheric indices. There are 44 stars in common between these works, which we will call sample A. For these stars, we have taken

isochrone ages from Edv93 and estimated chromospheric ages using equation (3) of Soderblom et al. (1991), which can be written as

$$\log t_{\text{ce}} = -1.50 \log R'_{\text{HK}} + 2.25 \quad (1)$$

where t_{ce} is in yr. This is equivalent to $R'_{\text{HK}} \propto t^{-2/3}$, and corresponds

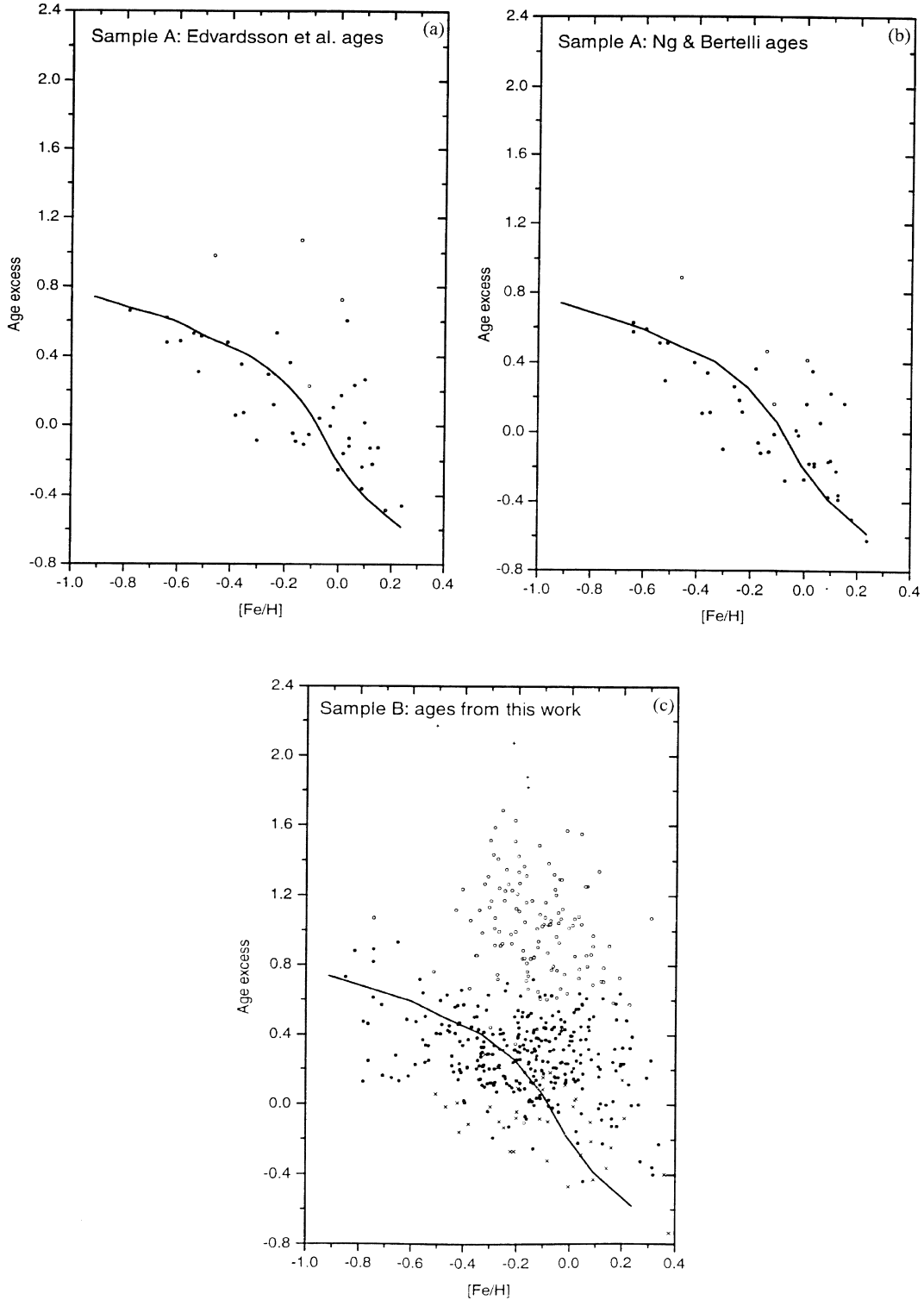


Figure 1. Chromospheric age excesses as a function of [Fe/H]. (a) Sample A (44 stars), using Edv93 ages. (b) Sample A using Ng & Bertelli (1998) ages. (c) Sample B (471 stars). Symbols are as follows: very active stars (plus signs), active stars (open circles), inactive stars (filled circles), and very inactive stars (crosses).

to the best power-law fit to their data. It should be noted that the use of any of the relations suggested by Soderblom et al. (1991) would produce essentially the same results. In Fig. 1 we show the difference between the isochrone (t_{is}) and chromospheric (t_{ce}) ages, or *age excess*, as a function of the metallicity $[\text{Fe}/\text{H}]$,

$$\Delta(\log t) = \log t_{\text{is}} - \log t_{\text{ce}}. \quad (2)$$

We have used open circles for active stars ($\log R'_{\text{HK}} \geq -4.75$), and filled circles for inactive stars ($\log R'_{\text{HK}} < -4.75$, cf. Vaughan & Preston 1980). Note that, except for a few isolated points, there is a clear-cut relation between the age excesses and $[\text{Fe}/\text{H}]$, especially for the inactive stars, in the sense that the chromospheric ages are substantially lower than the isochrone ages for metal-poor objects, while the opposite occurs for metal-rich stars. The age excess is minimal for metallicities around solar.

Recently, Ng & Bertelli (1998) revised the Edv93 ages, incorporating new updated isochrones and absolute magnitudes from *Hipparcos* parallaxes. Fig. 1(b) takes into account these revised ages for the stars in sample A. Note that the scatter is somewhat lower, and the general trend of Fig. 1(a) is confirmed. The curve in Figs 1(a) and (b) corresponds to a third-order polynomial fitted to the inactive stars with ages by Ng & Bertelli (1998).

Aside from sample A, we have built an independent sample with 730 stars (hereafter sample B) by the intersection of the surveys from HSDB and Soderblom (1985) with the *uvby* catalogues of Olsen (1983, 1993, 1994). The metallicity of each star in sample B was estimated from the calibrations of Schuster & Nissen (1989). The metallicities for three stars redder than $(b - y) = 0.580$ were given by the calibration of Olsen (1984) for K2–M2 stars. In order to obtain the colours δm_1 and δc_1 , we have adopted the standard curves $(b - y) \times m_1$ and $(b - y) \times c_1$ given by Crawford (1975) for late F and G0 dwarfs, and by Olsen (1984) for mid- and late G dwarfs. The zero-age main-sequence (ZAMS) curve $(b - y) \times c_1$ was corrected as in Edv93 to allow for a dependence on $[\text{Fe}/\text{H}]$. Finally, $\log T_{\text{eff}}$ and ΔM_V (the absolute magnitude deviation above the ZAMS) were calculated by the calibrations presented by Olsen (1984). Since all stars in Sample B are expected to be located within 50 pc around the Sun, no correction for reddening was applied to the photometric indices.

In order to obtain the ages, theoretical isochrones from the work of Vandenberg (1985) were used. He presents grids of isochrones for metallicities $[\text{Fe}/\text{H}] = 0.0, -0.23, -0.46, -0.76$ and -1.00 , and He abundance $Y = 0.25$. Following the general practice in isochrone age determinations (e.g., Twarog 1980; Soderblom et al. 1991; Edv93), we transformed his isochrones in the plane $M_V \times \log T_{\text{eff}}$ to the plane $\Delta M_V \times \log T_{\text{eff}}$, using tabulated ZAMS curves given by Vandenberg (1985). Also, we have shifted the resulting isochrones by $\delta \log T_{\text{eff}} = -0.009$ as Vandenberg's models seem to be slightly too hot for disc stars, according to Edv93. We plotted each star from sample B in these five sets of isochrone grids. An age for the star was estimated by graphic interpolation in each grid. A first- or second-order polynomial was fitted to these ages for each star. The stellar age was found by applying the photometrically calculated $[\text{Fe}/\text{H}]$ to the polynomial. We have estimated ages only for the stars which had ages in at least two sets of grids, amounting to 471 stars.

Table A1 (see Appendix A) shows the 730 stars of sample B. In the first column we give the HD number. The next columns list, respectively, $\log R'_{\text{HK}}$, $[\text{Fe}/\text{H}]$, $\log T_{\text{eff}}$, ΔM_V , the isochrone logarithmic age, the chromospheric logarithmic age, and the age excess. The average errors in $\log T_{\text{eff}}$ and ΔM_V can be estimated from the calibrations we have used as $\sigma(\log T_{\text{eff}}) \sim \pm 0.011$ and

$\sigma(\Delta M_V) \sim 0.29$ mag. These errors imply an age uncertainty of 1.5 to 3 Gyr for the hotter and cooler stars, respectively. An error of about 0.16 dex in the metallicity calibration further increases the age uncertainty by about 1 Gyr.

In Fig. 1(c), we show the age excesses for sample B. As well as the symbols used in the previous panels, we use plus signs for very active stars ($\log R'_{\text{HK}} > -4.20$) and crosses for very inactive stars ($\log R'_{\text{HK}} < -5.10$). The same general trend arises in this figure: metal-poor stars show lower chromospheric ages [$\Delta(\log t) > 0$], while metal-rich stars show higher chromospheric ages [$\Delta(\log t) < 0$]. The curve fitted to sample A is included for comparison. It can be seen that a number of stars deviate from the general trend, especially active and very active stars, which can also be observed in Fig. 1(a). On the other hand, almost all the stars which follow the observed trend between age excess and $[\text{Fe}/\text{H}]$ have $\log R'_{\text{HK}} < -4.75$, and are inactive or very inactive stars. In Fig. 1(b) the same trend can be observed, although the behaviour of the active stars is not as clear. In the next section, we will try to understand why these two classes of stars, which were defined according to the chromospheric activity level, present different trends regarding their age excesses.

The data from sample A is more accurate than the data from sample B, since the photometric calibrations for F and early G dwarfs are better defined than for late G dwarfs. Moreover, we used a spectroscopic metallicity in sample A, and a photometric one in sample B. This is reflected in the higher scatter observed in Fig. 1(c) as compared with Figs 1(a,b). Note that the scatter observed in Fig. 1 is probably real, as the chromospheric ages depend on the CE index R'_{HK} which is expected to vary on small time-scales, as a result of the stellar magnetic cycle. For example, for the Sun a variation in the range $-5.10 \leq \log R'_{\text{HK}} \leq -4.75$ is observed (cf. HSDB). Therefore, we decided to use sample B only as an independent check of the results of Figs 1(a,b), and derived a correction to the chromospheric age on the basis of the results shown in Figs 1(a,b). In this case, the *corrected chromospheric age* can be written as

$$\log t_{\text{ce}}(\text{corrected}) = \log t_{\text{ce}} + \Delta(\log t) \quad (3)$$

where

$$\Delta(\log t) = -0.193 - 1.382[\text{Fe}/\text{H}] - 0.213[\text{Fe}/\text{H}]^2 + 0.270[\text{Fe}/\text{H}]^3, \quad (4)$$

which corresponds to the polynomial fit in Fig. 1(b). Note that this correction should be added to the logarithm of the chromospheric age, given in yr. This correction can be applied to chromospheric ages derived from published CE–age calibrations (Soderblom et al. 1991; Donahue 1993, as quoted by HSDB) for $\log R'_{\text{HK}} < -4.75$ in the range $-1.2 < [\text{Fe}/\text{H}] < +0.4$.

We checked in the catalogue of Cayrel de Strobel et al. (1997) for the metallicities of the stars used by Soderblom et al. (1991) for the building of the CE–age relation. The mean metallicity of these stars is -0.05 dex, with a standard deviation of 0.16 dex. Referring to Figs 1(a) and (b), we can see that for $[\text{Fe}/\text{H}] = -0.05$ we have $\Delta(\log t) \approx 0$, which reinforces our conclusion that the published CE–age calibrations are valid for solar metallicity stars only.

Another evidence favouring our conclusions is presented in Fig. 2, where we plot the chromospheric emission index for the stars of sample A as a function of the calcium abundance $[\text{Ca}/\text{H}]$ taken from Edv93. Again, for the inactive stars, the figure shows that the calcium-rich stars, which are expected to be also metal-rich and young, have generally lower CE indices. This can be explained by the fact that these stars have stronger Ca features, which leads to a lower R'_{HK} and correspondingly higher chromospheric ages, as

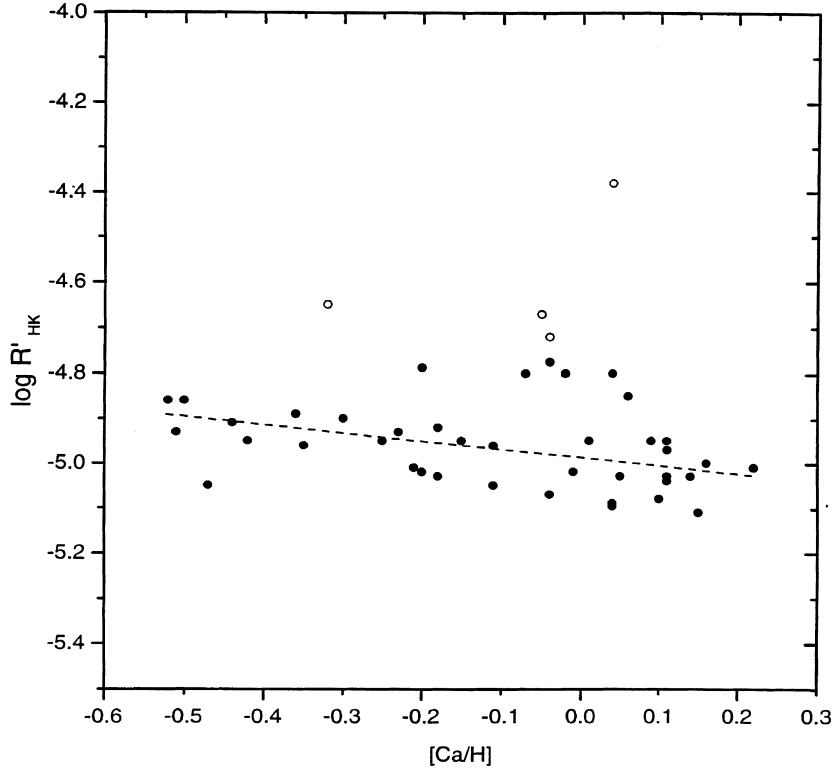


Figure 2. CE index as a function of the Ca abundances for the stars in Sample A. The values of $[Ca/H]$ are from Edv93. Open circles: active stars; filled circles: inactive stars.

observed in Fig. 1(a). Inversely, calcium-poor stars show higher chromospheric indices, which is mainly a result of their weaker Ca spectral features.

3 METALLICITY DISTRIBUTIONS ACCORDING TO CE LEVEL

Vaughan & Preston (1980) noted that solar neighbourhood stars could be divided into two populations, namely active and inactive stars, hereafter referred to as AS and IS, respectively. The separation between these populations is made by the so-called Vaughan–Preston gap, located around $\log R'_{HK} = -4.75$, which is a region of intermediate activity containing very few stars. Recently, HSDB showed that the Vaughan–Preston gap is a transition zone instead of a zone of avoidance of stars. Moreover, they showed that two additional populations seem to exist: the very active stars (VAS; $\log R'_{HK} > -4.20$) and the very inactive stars (VIS; $\log R'_{HK} < -5.10$).

It is interesting to see whether any trends in the chemical composition of these four groups exist. At first glance, on the basis of the existence of a deterministic CE–age relation (Soderblom et al. 1991), and of the age–metallicity relation, we would expect a CE–metallicity relation to exist. The dependence on $[Fe/H]$ of the CE–age relation, discussed in the previous section, could hinder or mask such a CE–metallicity relation, and our results could in principle show whether or not that dependence is real.

Fig. 3 shows the $[Fe/H] \times \log R'_{HK}$ diagram for the 730 stars of sample B. The vertical dashed lines separate the four populations according to their activity level. Contrary to the argument presented in the previous paragraph, there seems to be no significant CE–metallicity relation. Moreover, it is clear that the metallicity

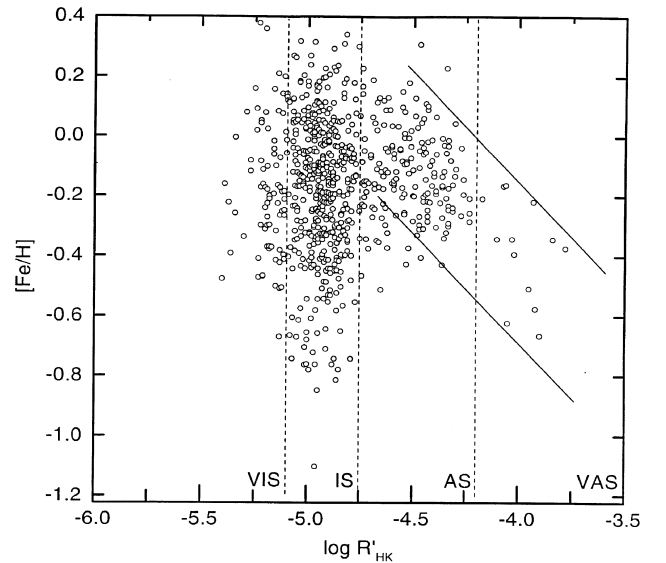


Figure 3. $[Fe/H] \times \log R'_{HK}$ diagram for the 730 stars of sample B. The vertical dashed lines separate the four populations. The solid lines mark an apparent ‘activity strip’ where the AS and VAS are mainly located.

distribution of the four groups are very different from each other. This is shown more clearly in Fig. 4, where we compare their metallicity distributions with the solar neighbourhood metallicity distribution (Rocha-Pinto & Maciel 1996).

It can be seen from Fig. 4 that the metallicity distribution of the IS is very similar to the solar neighbourhood standard distribution, suggesting that the IS sample represents the stars in our vicinity

very well. This is not surprising, since about 70 per cent of the stars in the solar neighbourhood are inactive (cf. HSDB). The other metallicity distributions show some deviations from the standard distribution, as follows:

(i) The paucity of metal-poor stars in the VIS group is peculiar, as these should be the oldest stars in the Galaxy, according to their low CE level, and the oldest stars are supposed to be metal-poor if the chemical evolution theory is correct.

(ii) The lack of metal-poor stars is even more pronounced in the AS group, and the transition from the IS to the AS at the Vaughan–Preston gap suggests an abrupt change in the metallicity distribution of these stars. The AS have metallicities in a narrow range from about -0.35 dex to $+0.15$ dex, with an average around -0.15 dex. It is interesting to note that the majority of stars with $[\text{Fe}/\text{H}] > +0.20$, which should be very young according to the chemical evolution, are not AS (young stars according to published CE–age relations), but appear amongst the VIS and the IS (old stars according to CE level).

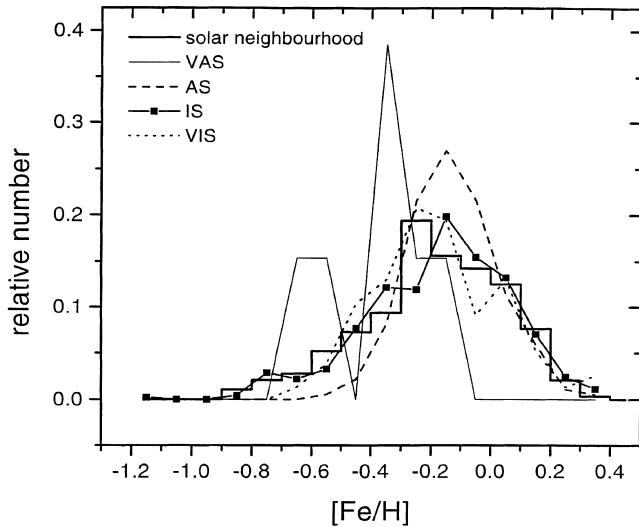


Figure 4. Metallicity distributions of the four populations compared to the solar neighbourhood metallicity distribution from Rocha-Pinto & Maciel (1996).

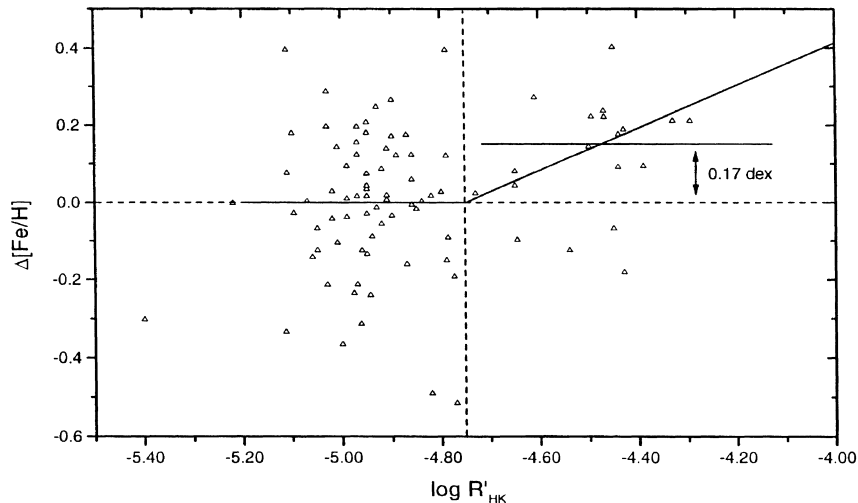


Figure 5. The difference between the spectroscopic and photometric metallicity $[\text{Fe}/\text{H}]$ as a function of the CE level.

(iii) There are very few VAS, but their metallicities seem to be lower than the metallicities of the AS. From Fig. 3 it can be seen that the VAS, together with the AS, appear to be located mainly in a well-defined ‘activity strip’ on the $[\text{Fe}/\text{H}] \times \log R'_{\text{HK}}$ diagram, which we have marked by solid lines in this figure.

The nature of the VIS and the VAS has already been treated by HSDB. The VIS are probably stars experiencing a phase similar to the Maunder Minimum observed in the Sun. The paucity of metal-poor stars in the VIS group reinforces this conclusion, by ruling out the hypothesis of old ages for these stars.

The VAS seem to be formed mainly by close binaries. HSDB have confirmed that many of the VAS in their sample are known to be RS CVn or W UMa binaries, and have been detected by ultraviolet and X-ray satellites. In fact, a CE–age relation is not supposed to be valid for binaries (at least close binaries), since these stars can keep high CE levels, even at advanced ages, by synchronizing their rotation with the orbital motion (Barrado et al. 1994, Montes et al. 1996). It is possible that not all VAS are close binaries; some of them could instead be very young stars. It is significant that the BY Draconis systems are composed of either close binaries or very young field stars (Fekel, Moffett & Henry 1986), and that also the only difference between BY Dra and RS CVn stars is that BY Dra have later spectral types (Eker 1992). However, taking into account their metallicity distribution, which shows no stars with $[\text{Fe}/\text{H}] > -0.10$ dex, it would appear that the close binaries hypothesis is more appealing, as very young stars should be metal-rich.

Nevertheless, the situation is not so clear. The low $[\text{Fe}/\text{H}]$ content of the VAS could be partially responsible for the high $\log R'_{\text{HK}}$ indices in these stars, for the reasons explained in Section 2. On the other hand, it is also known that a high level of chromospheric activity can decrease the m_1 index by filling up the cores of the metallic lines, simulating a lower $[\text{Fe}/\text{H}]$ content (Giampapa, Worden & Gilliam 1979; Basri, Wilcots & Stout 1989). Giménez et al. (1991) have shown that the m_1 deficiency in active systems like RS CVn stars is severe and can substantially affect the values of the photometrically derived stellar parameters. It should be recalled that even the Sun, which is an inactive star, would look 35 per cent more metal-poor if observed in a region of activity (Giampapa et al. 1979). Thus, it is very likely that the low metallicity of the VAS is only an effect of their highly active chromospheres, and not an indication of older age. A similar conclusion was recently reached

by Favata et al. (1997) and Morale et al. (1996) based on photometric and spectroscopic studies of a sample of very active K-type stars.

4 THE ORIGIN OF THE ACTIVITY STRIP

It is now possible to make two hypotheses in order to understand the activity strip and other trends on the $[\text{Fe}/\text{H}] \times \log R'_{\text{HK}}$ diagram.

(a) Stars with lower metallicities should present higher apparent chromospheric indices $\log R'_{\text{HK}}$, since the Ca lines are shallower in the spectra of metal-poor stars (see Fig. 2). This could produce an anticorrelation between $[\text{Fe}/\text{H}]$ and $\log R'_{\text{HK}}$.

(b) The chromospheric activity affects the photometric index m_I in such a way that the larger the CE level in a star, the more metal-poor this star would appear (Giménez et al. 1991). This can also

produce an anticorrelation as seen in the activity strip beyond the Vaughan–Preston gap.

The first hypothesis can account well for the deviations between isochrone and chromospheric ages seen amongst the IS [Figs 1(a) and (b)]. For the active stars, this is not as obvious, and Fig. 1 suggests that these stars require different corrections, as compared to the inactive stars. If all active stars were close binaries of RS CVn or BY Dra types, this could also explain the activity strip. In that case, close binaries with $[\text{Fe}/\text{H}] \geq +0.0$ would not be found amongst the VAS, but in the AS group. However, we have found no preferred region on the $[\text{Fe}/\text{H}] \times \log R'_{\text{HK}}$ diagram where the known resolved binaries (not only close binaries) in our sample B are located. Moreover, it is well known that many AS stars are not binaries.

The second hypothesis is particularly suitable for explaining the

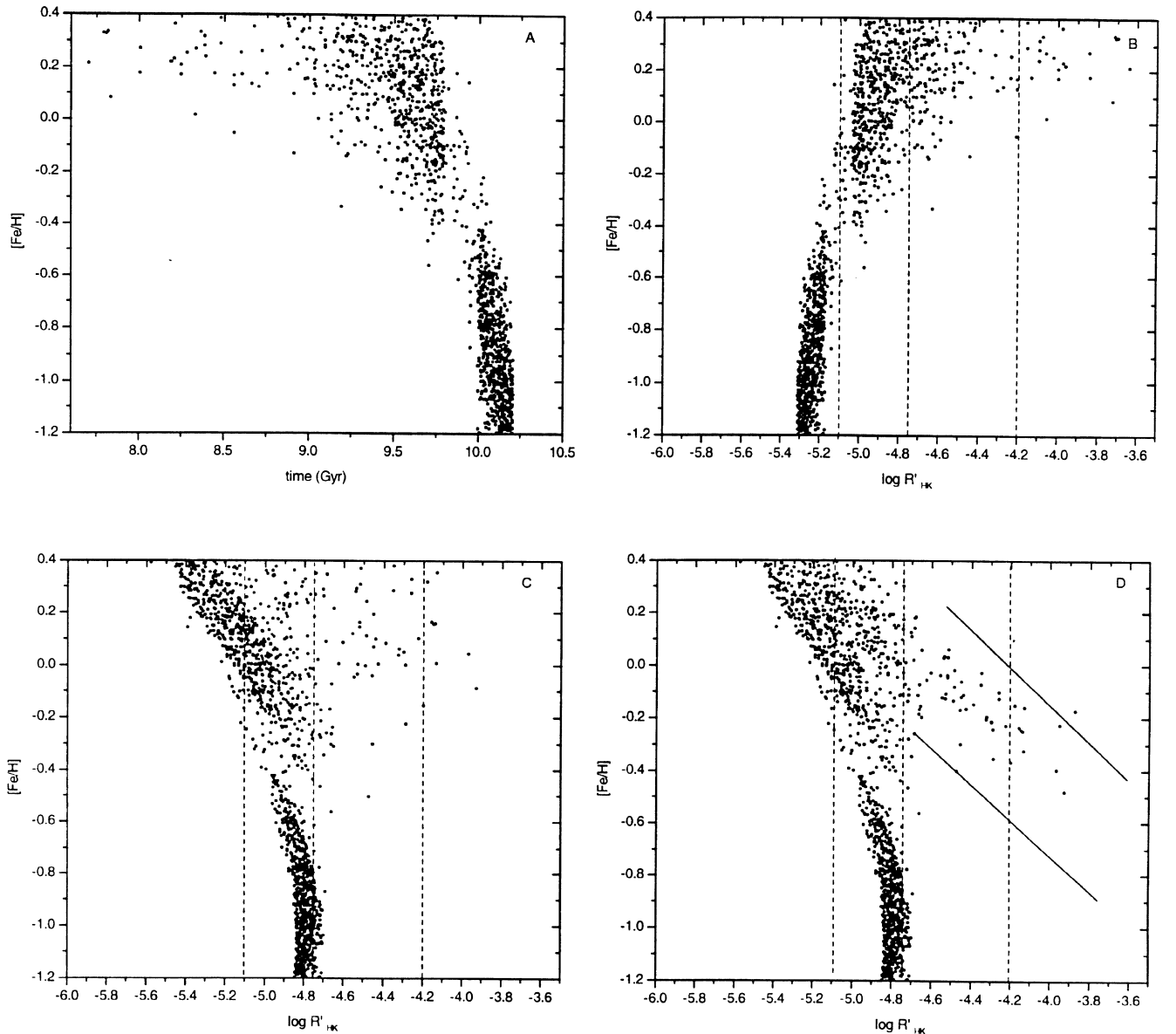


Figure 6. Simulation of the $[\text{Fe}/\text{H}] \times \log R'_{\text{HK}}$ diagram for a set of 1750 fictitious stars: (a) age–metallicity relation assuming a constant stellar birthrate; (b) CE–metallicity diagram assuming no metallicity dependence of the $\log R'_{\text{HK}}$ index; (c) CE–metallicity diagram adopting equation (4), and correcting the metallicity of the active stars according to equations (5); (d) the same as panel (c), but the metallicity is corrected using equation (6).

activity strip, since it does not require all active stars to be binaries. In fact, the shape of the $\log R'_{\text{HK}} \times [\text{Fe}/\text{H}]$ diagram, showing a quite abrupt change in the $[\text{Fe}/\text{H}]$ distribution at the Vaughan–Preston gap, suggests that different processes are at work on both sides of the gap.

To test hypothesis (b), we have searched for spectroscopic metallicities in Cayrel de Strobel et al. (1997) for the stars in sample B. For the sake of consistency, we have used the most recent determination of $[\text{Fe}/\text{H}]$ for stars having several entries in this catalogue. Note that the spectroscopic metallicity is not likely to be affected by the chromospheric activity, and could serve as a tool to check whether our photometrically derived $[\text{Fe}/\text{H}]$ abundances are underestimated.

In Fig. 5, we show the difference $\Delta[\text{Fe}/\text{H}]$ between the spectroscopic and the photometric metallicities as a function of $\log R'_{\text{HK}}$. As in the previous figures, two distinct trends can be seen here. For IS ($\log R'_{\text{HK}} < -4.75$), the scatter in $\Delta[\text{Fe}/\text{H}]$ is high but the stars appear very well distributed around the expected value

$\Delta[\text{Fe}/\text{H}] \approx 0$. A Gaussian fit to the $\Delta[\text{Fe}/\text{H}]$ distribution for these stars gives a mean $\langle \Delta \rangle \approx 0.03$ dex and standard deviation $\sigma \approx 0.13$ dex. Such scatter is very likely the result of observational errors as well as of the inhomogeneity of the spectroscopic data, which was taken from several sources. For the AS ($\log R'_{\text{HK}} > -4.75$), the data clearly show that there is a *positive* $\Delta[\text{Fe}/\text{H}]$, with few deviating points. According to a Kolmogorov–Smirnov test, the hypothesis that the $\Delta[\text{Fe}/\text{H}]$ distributions are the same for both inactive and active stars can be rejected to a significance level lower than 0.05.

The paucity of points in this part of the diagram makes the relation between $\Delta[\text{Fe}/\text{H}]$ and $\log R'_{\text{HK}}$ somewhat confusing. As a first approximation, we will assume that $\Delta[\text{Fe}/\text{H}]$ is independent of the CE level, so that it can be written as

$$\Delta[\text{Fe}/\text{H}] = 0.17, \quad \log R'_{\text{HK}} > -4.75 \quad (5a)$$

$$= 0, \quad \log R'_{\text{HK}} \leq -4.75 \quad (5b)$$

This correction has been applied to the active stars of sample B to

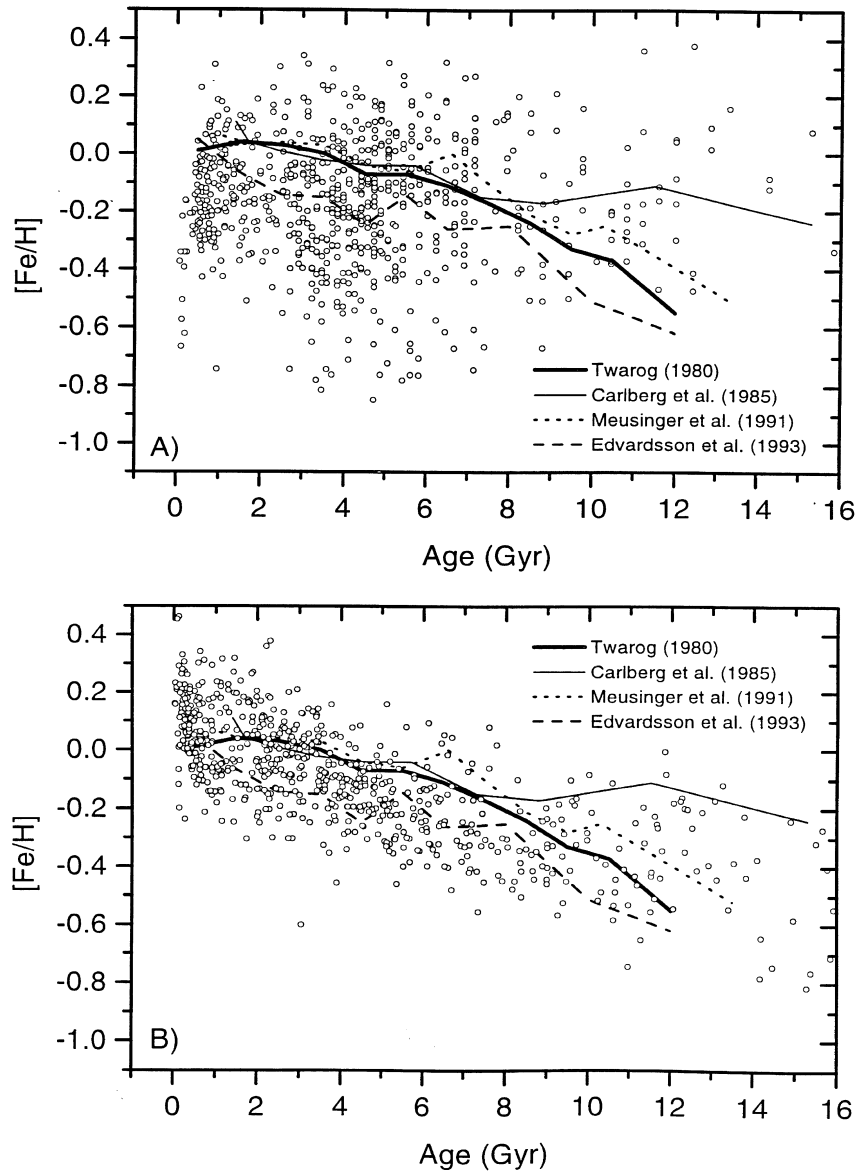


Figure 7. (a) Uncorrected and (b) corrected age–metallicity relation for sample B. Also shown are some AMR from the literature.

find the expected metallicity for these stars. The value 0.17 dex corresponds to the mean $\Delta[\text{Fe}/\text{H}]$ of the active stars in Fig. 5, excluding the four stars with negative $\Delta[\text{Fe}/\text{H}]$. If these stars are included, the mean $\Delta[\text{Fe}/\text{H}]$ decreases down to about 0.11 dex.

From a more physical point of view, it is expected that $\Delta[\text{Fe}/\text{H}]$ increases as the CE level increases (Giménez et al 1991; Favata et al. 1997). Therefore, we have fitted a straight line by eye again excluding the deviating stars, and assuming that $\Delta[\text{Fe}/\text{H}] \approx 0$ for $\log R'_{\text{HK}} \leq -4.75$. The obtained expression for this approximation is

$$\Delta[\text{Fe}/\text{H}] = 2.613 + 0.550 \log R'_{\text{HK}}, \quad (6)$$

as can be seen by the straight line in Fig. 5.

To explain the shape of the $[\text{Fe}/\text{H}] \times \log R'_{\text{HK}}$ diagram, we have made a simulation of the diagram in Fig. 3, using a set of 1750

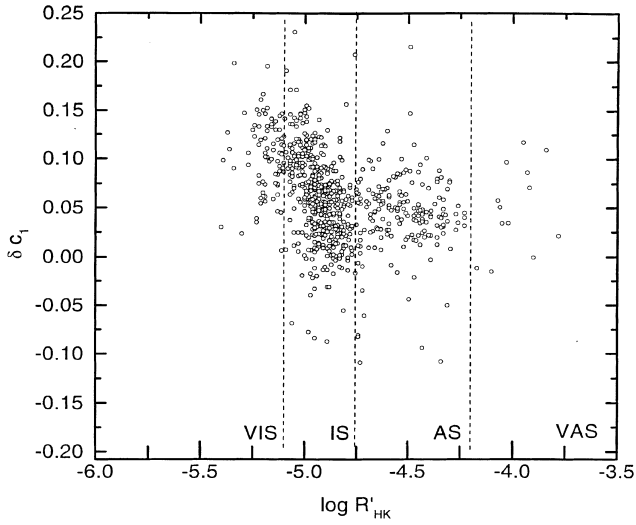


Figure 8. $\delta_{c1} \times \log R'_{\text{HK}}$ diagram for sample B. The δ_{c1} index can be regarded as a rough age indicator for our sample.

Table 1. Spatial velocities for VAS and AS in sample B.

HD	$\log R'_{\text{HK}}$	U	V	W	HD	$\log R'_{\text{HK}}$	U	V	W	HD	$\log R'_{\text{HK}}$	U	V	W
166	-4.33	-15	-23	-10	61994	-4.59	2	-23	-20	144872	-4.74	55	5	5
1835 A	-4.44	-33	-13	0	65721	-4.67	-44	-9	-26	147513 A	-4.52	17	-3	-1
4391	-4.55	-22	0	7	72905	-4.33	10	0	-10	150706	-4.59	20	-4	-13
10780	-4.61	-23	-15	-4	74576	-4.31	-26	-9	-1	152391	-4.39	84	-108	10
10800	-4.60	-11	-6	-10	74842	-4.58	27	-9	-21	160346	-4.71	19	-1	12
11131 B	-4.47	20	3	-5	82106	-4.43	-36	-13	0	165185	-4.43	13	5	-9
13445	-4.74	-109	-80	-24	88742	-4.69	-31	-44	-1	165401	-4.65	-83	-84	-38
17051	-4.65	-27	-15	-8	88746 A	-4.70	-44	-6	-1	181321	-4.31	-13	-5	-7
17925	-4.30	-15	-16	-11	101501	-4.50	7	-15	-4	189087	-4.63	-34	-14	5
20630	-4.45	-22	-4	-4	103431	-4.68	-70	-38	-12	189931	-4.64	-44	-63	-5
20766	-4.65	-63	-42	13	110010	-4.47	-8	-21	-13	196850	-4.64	-1	-23	-34
22049	-4.47	-3	8	-20	110833	-4.72	-21	-24	13	202628	-4.73	-11	1	-27
25680	-4.54	-25	-15	-7	115043	-4.43	15	3	-8	203244	-4.39	1	9	-23
30495	-4.54	-23	-9	-3	120237 A	-4.75	-49	-60	-5	205905	-4.55	-40	-15	-15
36435	-4.44	12	-3	-19	124580	-4.54	11	0	-16	206860	-4.42	-13	-20	-8
37394 A	-4.43	-12	-21	-13	128165	-4.74	-21	7	11	209100	-4.56	-78	-41	3
41700 C	-4.35	-35	-11	-15	129333	-4.23	-7	-35	-3	216803	-4.27	-6	-9	-11
42807	-4.44	3	-25	-6	130948	-4.45	3	7	-6	219709 A	-4.62	-18	-40	-15
53143	-4.52	-24	-17	-15	131582 A	-4.73	-73	-71	18	220182	-4.41	-56	-15	-2
58830	-4.49	5	15	21	131977	-4.49	46	-21	-31	222335	-4.73	-2	-39	6
59967	-4.36	-11	-4	-7	134319	-4.33	-33	-15	-1					

fictitious stars. This set was built in a similar fashion to that described in Rocha-Pinto & Maciel (1997), using a constant stellar birthrate and a cosmic scatter in $[\text{Fe}/\text{H}]$ of 0.20 dex. In Fig. 6(a) we show the age–metallicity relation for this set of stars. Note that this figure is shown for illustrative purposes only, and we have made no attempts to use a relation closer to the real solar neighbourhood relation. This age–metallicity relation is transformed into a CE– $[\text{Fe}/\text{H}]$ relation in Fig. 6(b), using equation (1). This would be the shape of the $[\text{Fe}/\text{H}] \times \log R'_{\text{HK}}$ diagram if a CE–age relation and an age–metallicity relation exist, and if hypotheses (a) and (b) above were not valid. It can be seen that Fig. 6(b) does not reproduce the observed trends of the diagram of Fig. 3. In Fig. 6(c), we show the same diagram assuming that the ages have an excess $\Delta(\log t)$ relative to the chromospheric ages, as given in equation (4), and that the metallicities of the AS and VAS have a deficiency of $\Delta[\text{Fe}/\text{H}]$ as given by equations (5). Fig. 6(d) is similar to Fig. 6(c), except that equation (6) is used instead of equations (5). In Figs 6(b–d), the vertical dashed lines separate the four populations according to CE level, as in Fig. 3. Fig. 6(c) shows a clear progress in reproducing Fig. 3 as compared with Fig. 6(b), and Fig. 6(d) can in fact reproduce fairly well the trends of the observed CE–metallicity diagram of Fig. 3. Note that all old metal-poor stars in Fig. 6(b) look more active, that is, younger, in Fig. 6(d). Also, some young metal-rich stars are shifted to the VIS group in agreement with the observations. The activity strip beyond the Vaughan–Preston gap is also very well reproduced in Fig. 6(d). Note that Fig. 6(c) does not reproduce the activity strip, suggesting that equation (6) is physically more meaningful than equations (5).

Unfortunately, there are no calibrations for stellar parameters in chromospherically active stars, which would make it possible to check whether equation (6) gives the right corrections. However, the good agreement between our simulations and Fig. 3 suggests that our procedure to correct the photometric $[\text{Fe}/\text{H}]$ is reasonably good.

Another illustration of the correction procedure proposed in this paper is presented in Fig. 7, where we show the uncorrected age–metallicity relation (AMR) for sample B (Fig. 7a), as well as the

obtained relation after our correction procedure has been applied (Fig. 7b). Also shown are four average relations from the literature. It can be seen that the uncorrected sample presents a very large scatter, so that stars of all metallicities can be found at almost all ages. On the other hand, the corrected sample shows a much better agreement with the tendency presented by all previous relations, yet preserving some scatter averaging 0.2 dex as observed. A full discussion of this age–metallicity relation will be the subject of a forthcoming paper.

5 THE CE–AGE RELATION FOR ACTIVE STARS

Although a CE–age relation exists amongst late-type dwarfs, its shape is not well defined. The main uncertainty seems to occur for stars beyond the Vaughan–Preston gap. Soderblom et al. (1991) have shown that the slope of the CE–age relation could be steeper for $\log R'_{\text{HK}} > -4.75$. This would dramatically affect the interpretation of the peaks in the chromospheric age distributions as a result of star formation bursts in our Galaxy (Barry 1988; Noh & Scalzo 1990; Rocha-Pinto & Maciel 1997).

The calibration of the CE–age relation for the active stars, using T_{eff} and M_V derived from photometry, is not as simple as for the inactive stars, since we do not know very well the extent to which the photometric indices are affected by the chromospheric activity. Consider the example shown in Fig. 8. In this plot we show a $\delta c_1 \times \log R'_{\text{HK}}$ diagram for all stars in sample B. The δc_1 index is a measure of the distance of the star from the ZAMS. In a sample with a narrow T_{eff} range, as is the case of a sample comprised only of G dwarfs, it is possible to roughly associate a high δc_1 with a greater age (lower $\log R'_{\text{HK}}$), and vice versa. If the AS are really very young they should have $\langle \delta c_1 \rangle \approx 0.0$, and δc_1 should become higher as lower $\log R'_{\text{HK}}$ values are considered. From Fig. 8, despite the scatter, we can see a clear relation between δc_1 and $\log R'_{\text{HK}}$ for the IS and probably also the VIS, as expected on the basis of the previous discussion. However, the AS group does not show δc_1 indices typical of a very young population, and there seems to be no continuity in the $\delta c_1 \times \log R'_{\text{HK}}$ relation for inactive and active stars. The plot even suggests that the active stars could be composed of stars with a variety of ages.

According to Giménez et al. (1991) and Favata et al. (1997), the c_1 index is less likely to be affected by the chromospheric activity than the m_1 index. However, in the calculation of δc_1 we have also made use of the stellar metallicity, to account for the [Fe/H] dependence of the ZAMS. This is probably the main reason for not finding $\langle \delta c_1 \rangle \sim 0.0$ for the active stars. If δc_1 is incorrect, then ΔM_V would also be miscalculated, and the isochrone ages found for these stars would give no information about the real stellar age. Moreover, the photometric metallicity of the star is needed to interpolate between the isochrones of different metallicities, which would be another source of errors. This would produce a systematic error towards greater ages for the active stars.

In view of these considerations, it is not surprising that most active stars deviate from the relation between age excess and [Fe/H] in Figs 1(a) and (c). Note that all single stars with $\log R'_{\text{HK}} > -4.75$ in fig. 8 from Soderblom et al. (1991) also have isochrone ages (ranging nearly from 2 to 4 Gyr) systematically greater than their ages from the calibration, which could be caused by some of these effects. Until we have photometric calibrations for the stellar parameters in active stars, we cannot use photometrically derived temperatures and magnitudes to obtain stellar ages. The best way to calibrate the CE–age relation beyond the Vaughan–Preston gap

would be to use only open clusters. These objects could have ages determined by isochrone fitting, a procedure which is not affected by the CE level of the cluster stars. However, these clusters are generally distant and their low-mass stars are quite faint to allow CE measurements (Soderblom et al. 1991). On the other hand, a sample of stars having T_{eff} and [Fe/H] calculated from their spectra, and M_V from their parallaxes, could have accurate isochrone ages. This is what happens in Fig. 1(b), where M_V is calculated from trigonometrical parallaxes. In this figure, the active stars follow more closely the age excess relation given by equation (4).

A mean age for a group of stars can also be determined on the basis of its kinematical properties. Soderblom (1990) has investigated the kinematics of about 30 AS, and has found a mean age of 1 to 2 Gyr for the group. Nevertheless, he has found some active stars with kinematics of old population stars. We decided to reinvestigate the kinematics of the active stars, using a larger data sample. We have searched for spatial velocities for each active star of sample B in Gliese & Jahreiß (1991) and Soderblom

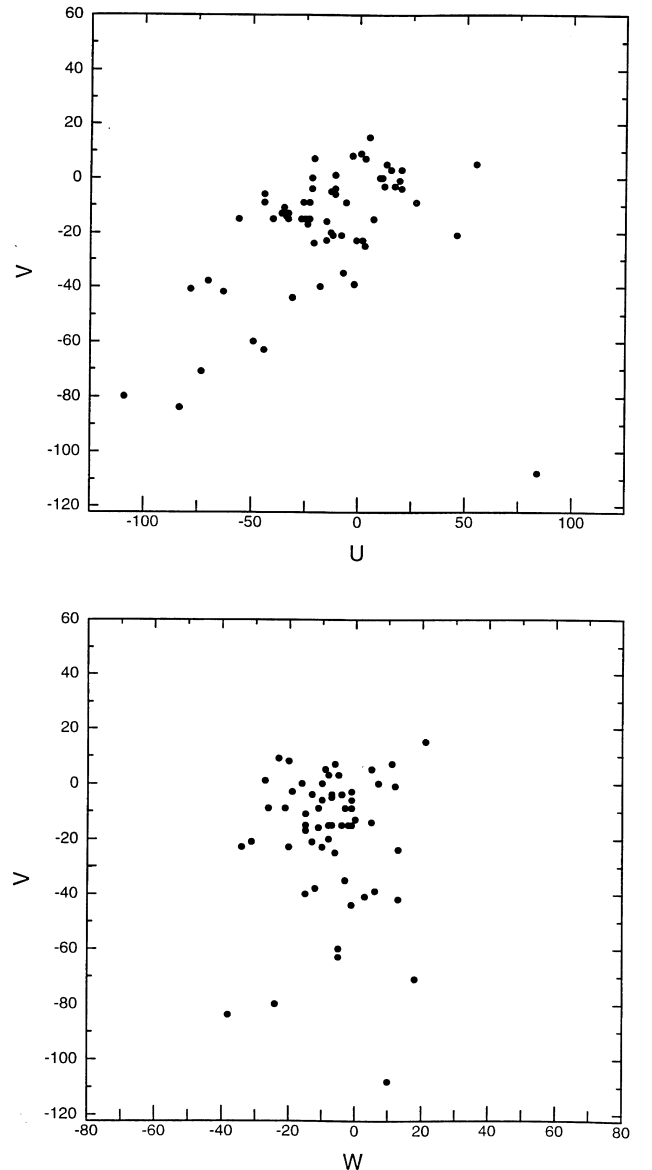


Figure 9. Spatial motions of 62 active stars listed in Table 1.

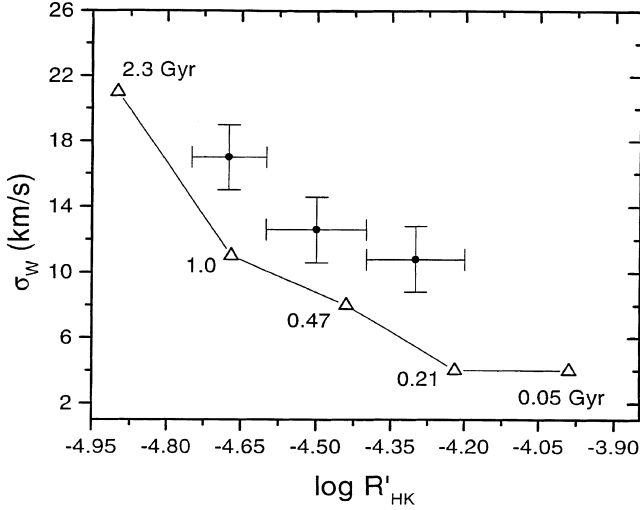


Fig. 10. Velocity dispersion σ_W as a function of $\log R'_{\text{HK}}$. The triangles show the σ_W –age relation (Wielen 1977), and we have used the CE–age calibration by Soderblom et al. (1991) to find the $\log R'_{\text{HK}}$ index for each age.

(1990). We have also calculated spatial velocities for 17 stars, from their radial and tangential velocities, proper motions and parallaxes, obtained from the SIMBAD data base, using the formulae from Johnson & Soderblom (1987). Table 1 lists 62 active stars with U , V and W velocities (km s^{-1}).

Fig. 9 shows the spatial motions of these stars. These panels are similar to those in Soderblom (1990). However, we have found several stars with the kinematics of old and intermediate-age populations. Some of these stars have $\log R'_{\text{HK}} \sim -4.75$, and could be inactive stars. The velocity dispersions σ_U , σ_V and σ_W are 36, 30 and 14 km s^{-1} , respectively, which indicates a mean age of 2 to 4 Gyr for the AS group according to Wielen (1977). However, an age of 1 to 2 Gyr would be found, in agreement with Soderblom (1990), if we disregard the stars with large velocities. It is still early to theorize upon the nature of such high-velocity active stars, and a larger sample is needed to allow firm conclusions.

We have also found a correlation between σ_W and $\log R'_{\text{HK}}$, which confirms the existence of a CE–age relation beyond the Vaughan–Preston gap. That is illustrated in Fig. 10. In this figure, the points with error bars are the calculated σ_W for three selected bins of our sample of active stars, and the triangles show the empirical σ_W –age relation according to Wielen (1977). The numbers near the triangles indicate a mean age for the stellar group with the corresponding σ_W . This relation was transformed into a σ_W – $\log R'_{\text{HK}}$ relation using the CE–age calibration by Soderblom et al. (1991). Note that the velocity dispersions for the active stars are systematically larger than the dispersions of their presumed coeval stars. This result suggests that the slope of the CE–age relation for the active stars is flatter than the slope in equation (3) of Soderblom et al., contrary to the relation that they propose to preserve the constancy of the star formation rate. However, this conclusion must be regarded with caution, as it is not founded on a large data base. In fact, considering only the open clusters in figure 8 from Soderblom et al., we would find a steeper slope. Much work is needed to understand the behaviour of the CE–age relation for active stars.

A program to measure spectroscopically T_{eff} , $[\text{Fe}/\text{H}]$, and abundance ratios in active stars is currently underway. Together with the new *Hipparcos* parallaxes, these data can cast some light on the discussion of the ages of the AS, and on the shape of the CE–age relation beyond the Vaughan–Preston gap.

ACKNOWLEDGMENTS

HJR-P thanks Gustavo F. Porto de Mello for an early suggestion of the relation between CE and age that has led to this work. We are indebted to Dr D. Soderblom for some comments on an earlier version of this paper. This research has made use of the SIMBAD data base, operated at CDS, Strasbourg, France. This work was supported by FAPESP and CNPq.

NOTE ADDED IN PROOF

After the acceptance of this paper, we learned about a recent preprint that investigates spectroscopic features of VAS (Soderblom, King & Henry 1998). They have found both single and binary stars amongst the VAS. For some of them it was possible to estimate $[\text{Fe}/\text{H}]$. Two of these stars (HD 37572 and HD 202917) are in our sample B. The difference $\Delta[\text{Fe}/\text{H}]$ of them are 0.324 and 0.224, respectively. These values agree fairly well with our equation (6), at the activity level of these stars ($\log R'_{\text{HK}}$ of -4.10 and -4.06 , respectively).

REFERENCES

- Barrado D., Fernández-Figueroa M. J., Montesinos B., de Castro E., 1994, *A&A*, 290, 137
 Barry D. C., 1988, *ApJ*, 334, 446
 Barry D. C., Cromwell R. H., Hege E. K., 1987, *ApJ*, 315, 264
 Basri G., Wilcots E., Stout N., 1989, *PASP*, 101, 528
 Carlberg R. G., Dawson P. C., Hsu T., Vandenberg D. A., 1985, *ApJ*, 294, 674
 Cayrel de Strobel G., Soubiran C., Friel E. D., Ralite N., François P., 1997, *A&A*, 124, 299
 Crawford D. L., 1975, *AJ*, 80, 955
 Donahue R. A., 1993, PhD thesis, New Mexico State Univ.
 Edvardsson B., Anderson J., Gustafsson B., Lambert D. L., Nissen P. E., Tomkin J., 1993, *A&A*, 275, 101 (Edv93)
 Eggen O. J., 1990, *PASP*, 102, 166
 Eker Z., 1992, *ApJS*, 79, 481
 Favata F., Micela G., Sciortino S., Morale F., 1997, *A&A*, 324, 998
 Fekel F. C., Moffett T. J., Henry G. W., 1986, *ApJS*, 60, 551
 Giampapa M. S., Worden S. P., Gilliam L. B., 1979, *ApJ*, 229, 1143
 Giménez A., Reglero V., de Castro E., Fernández-Figueroa M. J., 1991, *A&A*, 248, 563
 Gliese W., Jahreiß H., 1991, *Third Catalogue of Nearby Stars*. Astron. Rechen-Inst. Heidelberg
 Henry T. J., Soderblom D. R., Donahue R. A., Baliunas S. L., 1996, *AJ*, 111, 439 (HSDB)
 Johnson D. R. H., Soderblom D. R., 1987, *AJ*, 864
 Meusinger H., Reimann H.-G., Stecklum B., 1991, *A&A*, 245, 57
 Montes D., Fernández-Figueroa M. J., Cornide M., de Castro E., 1996, *A&A*, 312, 221
 Morale F., Micela G., Favata F., Sciortino S., 1996, *A&AS*, 119, 403
 Ng Y. K., Bertelli G., 1998, *A&A*, 329, 943
 Noh H.-R., Scalo J., 1990, *ApJ*, 352, 605
 Olsen E. H., 1983, *A&AS*, 54, 55
 Olsen E. H., 1984, *A&AS*, 57, 443
 Olsen E. H., 1993, *A&AS*, 102, 89
 Olsen E. H., 1994, *A&AS*, 104, 429
 Rocha-Pinto H. J., Maciel W. J., 1996, *MNRAS*, 279, 447
 Rocha-Pinto H. J., Maciel W. J., 1997, *MNRAS*, 289, 882
 Schuster W. J., Nissen P. E., 1989, *A&A*, 221, 65
 Skumanich A., 1972, *ApJ*, 171, 565
 Soderblom D. R., 1985, *AJ*, 90, 2103
 Soderblom D. R., 1990, *AJ*, 100, 204
 Soderblom D. R., Duncan D. K., Johnson D. R. H., 1991, *ApJ*, 375, 722
 Soderblom D. R., King J. R., Henry T. J., 1998, preprint (astro-ph/9803111)

Twarog B., 1980, ApJ, 242, 242
 VandenBerg D. A., 1985, ApJS, 58, 711
 Vaughan A. H., Preston G. W., 1980, PASP, 92, 385

Wielen R., 1977, A&A, 60, 263
 Wilson O. C., 1963, ApJ, 138, 832

APPENDIX A: STELLAR DATA FOR SAMPLE B

Table A1. Stellar data for sample B.

HD	log R ^{'HK}	[Fe/H]	log Teff	DMv	log tis	log tce	D(log t)												
20201	-4.93	-0.081	3.7771	0.6522	0.8633	0.6245	0.2388												
20407	-4.79	-0.4	3.7677	0.0153		0.6157													
20630	-4.45	0.058	3.7576	0.2924	0.896	-0.3544	1.2504												
20766	-4.646	-0.273	3.7570	0.2470	1.0354	0.2919	0.7435												
20782	-4.91	-0.097	3.7607	0.4993	1.0473	0.6063	0.441												
20794	-4.977	-0.245	3.7412	0.2390	1.1764	0.8074	0.369												
20807	-4.787	-0.289	3.7657	0.1952	0.8325	0.5493	0.2832												
21693	-4.87	0.015	3.7343	0.2039		0.555													
21938	-4.9	-0.415	3.7659	0.2846	1.0187	0.7884	0.2303												
22049	-4.469	-0.311	3.7174	-0.2620		-0.0133													
22484	-5.05	-0.042	3.7835	0.7860	0.7686	0.775	-0.0063												
23079	-4.94	-0.241	3.7730	0.3393	0.8927	0.7494	0.1433												
23249	-5.22	0.052	3.6808	0.3815		0.9544													
23576	-4.97	-0.006	3.7736	0.6557	0.8549	0.6268	0.2281												
24062	-5.25	0.158	3.7762	1.1675	0.6561	0.9068	-0.2507												
24085	-5	-0.012	3.7756	1.0327	0.8096	0.6765	0.133												
24224	-4.51	-0.074	3.7646	0.3682	0.9385	-0.116	1.0545												
24293	-4.93	-0.067	3.7579	0.5426	1.072	0.645	0.427												
24892	-5.2	-0.241	3.7296	0.3487		1.1394													
25388	-5.23	-0.411	3.7090	0.3376		1.2813													
25680	-4.54	-0.095	3.7622	0.5269	1.0346	-0.04	1.0746												
25740	-5.27	-0.083	3.7634	0.7747	1.0354	1.136	-0.1005												
26491	-4.95	-0.25	3.7586	0.5942	1.1775	0.77	0.4075												
26965	-4.944	-0.1	3.7260	-0.0402		0.6595													
27471	-5.1	-0.014	3.7655	0.9251	0.9469	0.8281	0.1188												
27631	-4.91	-0.327	3.7484	0.3765		0.756													
27905	-4.93	-0.188	3.7633	0.3331	0.9943	0.7	0.2944												
28187	-4.97	-0.432	3.7623	0.4336	1.26	0.705	0.555												
28388	-5.19	-0.372	3.7256	0.3940		1.2009													
28453	-5.06	-0.064	3.7799	1.1260	0.7818	0.8068	-0.025												
28701	-4.95	-0.463	3.7544	0.5295	1.301	0.675	0.626												
28904	-4.46	-0.406	3.7508	0.3867	1.266	0.0325	1.2335												
29231	-4.69	0.063	3.7318	0.1626	0.9777	0.1215	0.8562												
29303	-4.58	-0.143	3.7628	-0.1493		0.0754													
29813	-4.92	-0.028	3.7672	0.2765	0.8082	0.5691	0.2391												
30278	-4.95	-0.089	3.7368	0.2201	1.1281	0.6604	0.4677												
30495	-4.54	-0.005	3.7654	0.4267	0.8993	-0.1161	1.0154												
30649	-4.95	-0.545	3.7639	0.3741	1.177	0.675	0.502												
30774	-4.45	-0.039	3.7516	0.5485		-0.2648													
30966	-5.12	-0.252	3.7207	0.4389		1.0262													
31392	-4.75	0.0675	3.7300	0.1231		0.2364													
34599	-4.56	-0.046	3.7586	0.6021	1.0596	-0.0414	1.101												
34962	-4.47	-0.106	3.7400	0.1194	0.8567	-0.1676	1.0244												
35676	-4.48	0.028	3.7434	0.3374		-0.2656													
35854	-4.81	-0.242	3.6862	-0.1631		0.555													
35974	-5.06	-0.208	3.7745	0.8756	0.9763	0.9082	0.0682												
36435	-4.44	-0.196	3.7361	-0.0489		-0.1532													
36516	-4.9	-0.555	3.7652	0.5632	1.236	0.6	0.636												
36889	-5.16	-0.017	3.7589	0.9386	1.0269	0.9205	0.1064												
37213	-5.15	-0.502	3.7351	0.4535		0.975													
37572	-4.1	-0.344	3.7032	0.1196		-0.6943													
37655	-5.06	-0.167	3.7732	0.8773	0.9657	0.8808	0.0849												
37962	-4.83	-0.314	3.7555	0.3786	1.1682	0.6285	0.5397												
38230	-4.99	-0.081	3.7171	-0.0321		0.7145													
38283	-4.97	-0.111	3.7828	0.6711	0.8122	0.7065	0.1058												
38397	-4.26	-0.196	3.7713	0.3736	0.9175	-0.5041	1.4216												
38467	-5.07	0.27	3.7675	1.1762	0.525	0.855	-0.33												
38973	-4.88	-0.166	3.7764	0.7676	0.94	0.57	0.37												
39091	-4.97	-0.016	3.7785	0.7073	0.8041	0.6347	0.1694												
39427	-4.8	-0.281	3.7525	0.0583		0.564													
39601	-5.23	-0.473	3.7114	0.3345		1.3116													
39917	-4.05	-0.624	3.6937	0.5106		-0.675													
41004	-4.66	-0.092	3.6924	0.0426		0.19													
41330	-5.03	-0.436	3.7665	0.8555	1.1761	0.9939	0.1822												
42250	-5.01	0.025	3.7303	0.2439		0.6618													
42286	-4.89	-0.444	3.7087	-0.0116		0.7878													
42827	-4.59	-0.163	3.7755	0.5534	0.9191	0.1096	0.8094												
42490	-5.21	-0.469	3.7296	0.4002		1.065													
42807	-4.44	-0.145	3.7526	0.2083	0.9759	-0.194	1.1699												
43180	-4.77	-0.094	3.7630	0.5111	1.022	0.3941	0.6279												
43834	-4.94	0.099	3.7461	0.4197		0.4944													
44135	-4.33	-0.033	3.7649	0.2365	0.7782	-0.5107	1.2888												
44310	-5.07	-0.019	3.7241	-0.0526		0.7871													
44594	-4.92	0.043	3.7626	0.8451	0.9571	0.5119	0.4452												

Table A1 – *continued*

147513 A	-4.52	-0.125	3.7619	0.4694	1.041	0.03	1.011	
147873 A	-5.24	0.092	3.7868	1.4287	0.5211	0.9504	-0.4293	
157075 A	-4.87	-0.34	3.7910	0.8140	0.842	0.7033	0.1387	
161476 A	-4.92	-0.422	3.7625	0.5177	1.195	0.63	0.565	
16160 A	-4.97	-0.1	3.6787	-0.0188		0.6985		
164427 A	-4.95	0.11	3.7720	0.7662	0.7846	0.4997	0.2849	
178076 A	-4.53	-0.087	3.7361	0.0879		-0.066		
181199 A	-4.84	-0.289	3.7554	0.2191	1.029	0.6288	0.4002	
1835 A	-4.441	0.109	3.7617	0.6529	0.9138	-0.4226	1.3364	
185523 A	-4.9	0.002	3.7687	0.6102	0.8765	0.5154	0.3611	
197076 A	-4.93	-0.19	3.7625	0.4885	1.082	0.645	0.437	
212168 A	-4.89	-0.195	3.7694	0.8713	1.0314	0.6446	0.3868	
213240A	-5	0.182	3.7785	1.0274	0.621	0.75	-0.129	
214953 A	-4.89	-0.212	3.7811	0.8513	0.891	0.6558	0.2352	
217004 A	-5.19	-0.271	3.7534	0.8042	1.244	1.035	0.209	
219709 A	-4.62	-0.122	3.7625	0.4836	1.0362	0.1361	0.9001	
221231 A	-4.51	-0.035	3.7713	0.1335	0.5145	-0.1494	0.6639	
222668 A	-5.3	-0.338	3.7021	0.2939		1.3472		
223913A	-4.52	0.178	3.7770	0.0329		0.03		
22705 A	-4.33	-0.246	3.7734	0.3459	0.8998	-0.3265	1.2263	
25874 A	-4.93	-0.032	3.7568	0.5613	1.064	0.645	0.419	
32778 A	-4.87	-0.45	3.7582	0.0620		0.7607		
33473 A	-5.1	-0.058	3.7686	0.8554	0.9513	0.8622	0.0891	
37394 A	-4.43	-0.019	3.7168	-0.0067		-0.3227		
38392 B	-4.495	-0.202	3.6849	-0.0861		-0.0428		
38393 A	-4.774	0.123	3.8037	0.0851		0.2243		
4152 A	-4.67	-0.111	3.7364	0.1035	0.8267	0.2236	0.6031	
41700 C	-4.35	-0.341	3.7845	0.5591	0.8971	-0.2167	1.1138	
44120 A	-4.99	-0.185	3.7769	1.2283	0.8663	0.788	0.0783	
44665 A	-4.94	-0.089	3.7498	0.4617		0.6454		
45228 A	-5.2	-0.312	3.7406	0.4447		1.05		
45270 A	-4.32	-0.083	3.7688	0.3945	0.8982	-0.4846	1.3827	
5015 A	-5.03	-0.287	3.7891	1.4940	0.7177	0.9126	-0.1949	
6582 A	-4.99	-0.782	3.7370	0.1135	1.1864	1.0623	0.124	
65907 A	-4.79	-0.481	3.7723	0.5279	1.1106	0.6554	0.4552	
68978 A	-4.86	0.236	3.7766	0.3750	0.533	0.54	-0.007	
69565 A	-5.39	-0.162	3.6801	0.6278		1.3724		
74385 A	-4.55	-0.173	3.6903	-0.0190		0.0406		
75732 A	-4.97	0.104	3.6862	0.2977		0.535		
81485 A	-4.53	-0.093	3.7547	0.4361	1.099	-0.0611	1.1601	
82114 A	-5.105	0.013	3.7689	0.7882	0.892	0.908	-0.016	
82597 A	-5.13	-0.265	3.7613	0.6727	1.157	0.945	0.212	
88746 A	-4.7	-0.063	3.7391	0.1913	1.0378	0.2446	0.7933	

This paper has been typeset from a $\text{T}_E\text{X}/\text{L}^A\text{T}_E\text{X}$ file prepared by the author.